A Near-Edge X-ray Absorption Fine Structure Investigation of the Quasi-One Dimensional Organic Conductor $(TMTSF)_2PF_6$

K. Medjanik[†,*], A. Chernenkaya[‡,§], X. Kozina[‡], S. A. Nepijko[‡], G. Öhrwall[†], P. Foury-Leylekian[⊥], P. Alemany[‖], G. Schönhense[‡], E. Canadell[#] and J.-P. Pouget[⊥]

[†] Lund University, MAX IV Laboratory, 22100 Lund, Sweden

[‡] Institut für Physik, Johannes Gutenberg-Universität, 55099 Mainz, Germany

[§] Graduate School Materials Science in Mainz, 55128 Mainz, Germany

[⊥] Laboratoire de Physique des Solides, Université Paris-Sud, CNRS UMR 8502, 91405 Orsay, France

[‖] Departament de Ciència de Materials i Química Física and Institut de Química Teórica i Computacional (IQTCUB), Universitat de Barcelona, Martí i Franquès 1, 08028 Barcelona, Spain

[#] Institut de Ciència de Materials de Barcelona (ICMAB-CSIC), Campus de la UAB, 08193 Bellaterra, Spain

▪ ABSTRACT

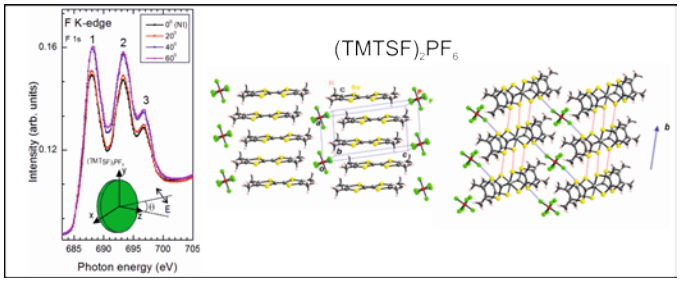

We present high-resolution near-edge X-ray absorption fine structure (NEXAFS) measurements at the P $L_{2/3}$-edges, F K-edge, C K-edge and Se $M_{2/3}$-edges of the quasi-one-dimensional (1D) conductor and superconductor $(TMTSF)_2PF_6$. NEXAFS allows probing the donor and acceptor moieties separately; spectra were recorded between room temperature (RT) and 30 K at normal incidence. Spectra taken around RT were also studied as a function of the angle (θ) between the electric field of the X-ray beam and the 1D conducting direction. In contrast with a previous study of the S $L_{2/3}$-edges spectra in $(TMTTF)_2AsF_6$, the Se $M_{2/3}$-edges of $(TMTSF)_2PF_6$ do not exhibit a well resolved spectrum. Surprisingly, the C K-edge spectra contain three well defined peaks exhibiting strong and non-trivial θ and temperature dependence. The nature of these peaks as well as those of the F K-edge spectra could be rationalized on the basis of first-principles DFT calculations. Despite the structural similarity, the NEXAFS spectra of $(TMTSF)_2PF_6$ and $(TMTTF)_2AsF_6$ exhibit important differences. In contrast with the case of $(TMTTF)_2AsF_6$, the F K-edge spectra of $(TMTSF)_2PF_6$ do not change with temperature despite stronger donor-anion interactions. All these features reveal subtle differences in the electronic structure of the TMTSF and TMTTF families of salts.

▪ INTRODUCTION

Since the discovery of organic superconductivity more than 35 years ago in the pressurized Bechgaard salt $(TMTSF)_2PF_6$,[1] a considerable amount of work has been devoted to the study of the cation radical $(TMTSF)_2X$ family of organic conductors and the sulfur analogues, the so-called Fabre salts, $(TMTTF)_2X$.[2] In these salts TMTSF is tetramethyl-tetraselenafulvalene,

TMTTF is tetramethyl-tetrathiafulvalene and X is a monovalent anion. These salts are low dimensional conductors due to an anisotropic structure made of (*a*,*b*) layers of donors whose zig-zag stacking along *a* leads to the formation of methyl group cavities in the perpendicular *c** direction which are filled with anions, X (Figure 1a). The charge transfer to the anion leaves one hole per two donor molecules leading to a quarter-filled band of holes. The 1D electronic properties of these salts are due to the preponderant overlap of the π-type HOMO (highest occupied molecular orbital) of the TMT(S/T)F donors along the stack direction, *a*.

Inside the methyl group cavities of these salts (Figure 1) each anion interacts with its surroundings by establishing upon cooling either short contact distances with neighboring Se/S donor atoms or H-bonds with close donor methyl groups. The relevance of these interactions is well documented in the salts incorporating non-centro-symmetric anions. The anions in these salts are disordered at RT but order upon cooling for entropy reasons. Their ordering process breaks the RT inversion symmetry of the cavity either by establishing one short Se···F contact out of two, as observed in $(TMTSF)_2ReO_4$,[3] or by setting O···H bonds with selected methyl groups, as observed in $(TMTSF)_2X$ (X = ClO_4 or NO_3).[4] In both cases the occurrence of anionic short contacts distorts the packing of donor stacks and the asymmetry of donor-anion contacts induces inter-donor charge transfer. All these features significantly modify the electronic structure of the $(TMTSF)_2X$ salts and the nature of their ground state.[5] In salts incorporating centro-symmetric anions such as X = PF_6, AsF_6 or SbF_6, no anion ordering transition occurs but the two types of coupling of the anion with the donor remain relevant. In particular, as we will see below, the donor-anion coupling has a key influence on the nature of the electronic ground state especially when charge degrees of freedom are involved.

The Bechgaard salt $(TMTSF)_2PF_6$ exhibits a complex thermal behavior at ambient pressure. At high temperature, due to the 1D nature of the electronic overlaps and to the

presence of sizeable electron-electron repulsions, $(TMTSF)_2PF_6$ behaves as a Tomonaga-Luttinger liquid.[6,7] Upon cooling, the electronic structure exhibits a 1D to 2D dimensional crossover around 100 K[8] which is achieved by de-confinement of the wave function in the *b* direction due to the sizeable overlap of the Se wave functions in the inter-stack directions (Figure 1b). Upon further cooling, the PF_6-librational motion in the methyl group cavity and the methyl group thermal rotational disorder freeze[9] below ~76 K and ~55 K respectively, causing a strengthening of the two types of donor-anion interactions considered above. Then, $(TMTSF)_2PF_6$ undergoes a spin density wave (SDW) metal-insulator transition at 12 K stabilized by the nesting of its open but sizably warped Fermi surface. Upon pressure the nesting condition deteriorates, the SDW ground state vanishes and when the metallic state is restored at low temperature $(TMTSF)_2PF_6$ exhibits superconductivity below about 1 K.[1]

The Fabre salts, $(TMTTF)_2X$, with weaker inter-stack S···S interactions are more 1D materials at ambient pressure. They exhibit a charge localization around 200 K, then a charge ordering transition around 100 K, both effects achieving a spin-charge decoupling. At low temperature, and for salts with centro-symmetric anions, the remaining spin degrees of freedom either couple antiferromagnetically or pair-up in singlet configurations leading to antiferromagnetic or spin-Peierls ground states, respectively (see for instance ref. 10). Under strong pressure the inter-stack interactions strengthen and the Fabre salts behave as the Bechgaard salts.

Although the phase diagram of salts with centro-symmetric anions can be rationalized[11] on the basis of the evolution of the quasi-1D donor electronic structure with pressure, donor substitution and size of the anions, recent NEXAFS and HAXPES (Hard X-Ray Photoelectron Spectroscopy) investigations of $(TMTTF)_2AsF_6$ and SbF_6 Fabre salts, respectively, have shown that the interaction between donors and anions is far from being negligible[12] and that anions play a subtle role in the stabilization of the charge ordering ground state.[12,13] In

particular the NEXAFS study showed unambiguously that the strengthening of F⋯S interactions upon cooling accompanies the charge localization. However at the present stage of our investigation it was not clear if the strengthening of the donor-anion interaction is simply due to the thermal contraction of the lattice or if it is a specific feature of the charge localization process.

In order to discriminate between these two possibilities we have performed a NEXAFS study of the unoccupied electronic levels of $(TMTSF)_2PF_6$ which exhibits a similar lattice contraction [14] as the Fabre salts[15] but, having a more 2D electronic structure, does not exhibit the charge localization phenomena at ambient pressure. In addition, this study should also probe the influence of the freezing of the PF_6-librational motion in the methyl group cavity and of the methyl group thermal rotational disorder on the electronic structure of $(TMTSF)_2PF_6$. Finally, since the NEXAFS study probes the unoccupied orbitals of both anion and donor, we will be able to evaluate how the donor-anion coupling influences the electronic structure of these salts.

In the following we report a combined experimental and theoretical study of the unoccupied electronic levels of $(TMTSF)_2PF_6$. In previous studies of molecular conductors (TTF-TCNQ,[32,35] $(TMTTF)_2AsF_6$[12]) we have found that a qualitative information concerning the nature, shape and relative ordering of the unoccupied electronic levels probed by NEXAFS is needed in order to have a clear microscopic interpretation of the NEXAFS results. Here we report NEXAFS measurements and a density functional theory (DFT) investigation of $(TMTSF)_2PF_6$ and we will compare the results with those of our previous study of $(TMTTF)_2AsF_6$.[12] The paper is organized as follows: experimental and computational methods are described in section II; NEXAFS spectra are presented in section III; the energy levels of PF_6, TMTSF and $(TMTSF)_2PF_6$ are discussed in section IV; then in section V the NEXAFS spectra will be discussed on the basis of the electronic structure

calculations and finally, in section VI, we summarize the results commenting the differences with the case of the Fabre salt $(TMTTF)_2AsF_6$.

- **METHODS**

Sample Preparation. $(TMTSF)_2PF_6$ single crystals were grown using the standard electrocrystallization procedure including THF (tetrahydrofuran) solvent which was also used to obtain the $(TMTTF)_2X$ crystals previously studied.[12,13] Two crystals obtained by this technique and with similar dimensions of about $1.5x1x0.1mm^3$ were studied. The largest crystal dimensions are those of the (*a*,*b*) donor layer with the longer direction being the stack direction, *a*, while the shortest direction is the interlayer direction *c**.

The samples were mounted in such a way that the (*a*, *b*) plane was put in contact with the sample holder. At normal incidence (θ = 0° to incoming x-ray beam; see inset in Figure 3a) the (*a*, *b*) plane is located in the plane of storage ring and oriented in such a way that the stack direction, *a*, is parallel to the electric field of the beam. By varying θ, the angle between the electric field and the surface plane was increasing accordingly, starting from pure s-polarized excitation (θ = 0°). Some data were also compared with those taken from pure TMTSF powder (from Sigma-Aldrich).

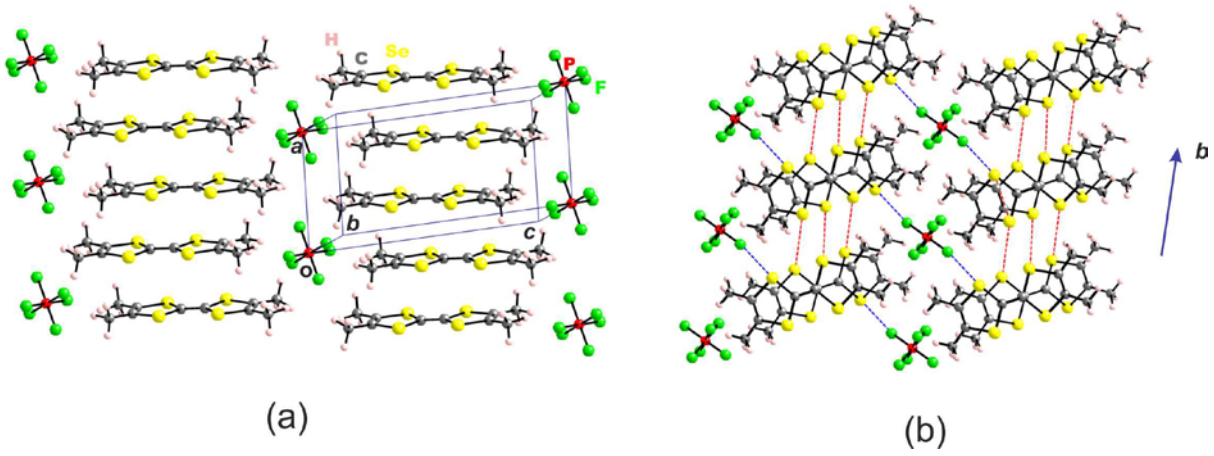

Figure 1. Structure of $(TMTSF)_2PF_6$. (a) Quasi-planar organic molecules stack along the *a*-axis and are separated by PF_6 anions in the *c**-direction. (b) Projection of $(TMTSF)_2PF_6$ structure along the stack direction. This projection shows in red the location of inter-stack interactions in the (*a*, *b*) donor layer through Se···Se short contacts and in blue the short contact Se···F donor –anion interactions.

Experimental Details. The experiments were performed at the synchrotron radiation I1011 beamline of the MAX II storage ring in Lund, Sweden.[16] The monochromator at I1011 delivers photons in the energy range of 130-1200eV and the radiation has a linear polarization in the plane of the storage ring. The degree of polarization is close to 100%. Spot size of the photon beam was $1x0.2mm^2$. NEXAFS spectra were collected at different angles of incidence θ and at different temperature in total electron yield (TEY) detection mode. Excitation energies were varied in intervals of typically 20 eV around the ionization energies. All temperature measurements (rate of temperature variation < 1K min^{-1}) were done in normal incidence mode. Due to the large depth (3-5 nm) probed by NEXAFS samples have been directly measured without any pre-cleaning procedure. No radiation damage was detected during 12 hours of measurements and the spot position was varied after each scan. NEXAFS spectra recorded from the two $(TMTSF)_2PF_6$ crystals investigated were identical.

Computational Details. The present calculations were carried out using a numerical atomic orbitals density functional theory (DFT) approach[17,18] which was developed for efficient calculations in large systems and implemented in the SIESTA code.[19-21] We have used the generalized gradient approximation (GGA) to DFT and, in particular, the functional of Perdew, Burke and Ernzerhof.[22] Only the valence electrons are considered in the calculation, with the core being replaced by norm-conserving scalar relativistic pseudopotentials[23]

factorized in the Kleinman-Bylander form.[24] We have used a split-valence double-ζ basis set including polarization orbitals with an energy shift of 10 meV for all atoms.[25] The energy cutoff of the real space integration mesh was 250 Ry. The Brillouin zone was sampled using a grid of (20×20×10) *k*-points[26] in the irreducible part of the Brillouin zone. Calculations for the "isolated" PF_6^- and TMTSF were carried out exactly as for the $(TMTSF)_2PF_6$ solid using an isolated species within a periodic box of 30×30×30 $Å^3$. In the case of PF_6^- a compensating uniformly distributed background charge amounting to one positive charge per unit cell was included. The experimental 4 K[14] and room temperature[27] crystal structures were used for the calculations.

- **NEXAFS SPECTRA OF $(TMTSF)_2PF_6$**

NEXAFS spectroscopy detects the resonant excitations from a selected core level (F 1s, C 1s, Se 3p, and P 2p in the case of $(TMTSF)_2PF_6$) into the unoccupied density of states above the Fermi level. Being a local probe, NEXAFS is able to probe both the electronically active TMTSF molecule (through C K- and Se $M_{2/3}$-edges) and the PF_6 anion (through F K- and P $L_{2/3}$-edges) separately. However our previous study of the Fabre salts revealed[12] that even when the emitter atom is located in the anion layer, information on the unoccupied wave-functions of the donor layer can be obtained because of the hybridization of TMTSF wavefunctions with those of the anion.

Angular dependent NEXAFS, which will be considered in part A below, provides pertinent information for a macroscopically ordered structure built with well oriented emitting entities. Owing to the zig-zag structure of the stacks (see Figure 1) $(TMTSF)_2PF_6$ is a perfect candidate for such investigations. The interpretation of the results should be strongly simplified because of the quasi-planar structure of TMTSF donors building the stacks. Thus

NEXAFS spectra were taken at θ = 0°, 20°, 40° and 60° impact angle between the electric field and the TMTSF surface, containing the stacking direction, *a*.

We report separately in parts A and B below the angular- and temperature-dependence of the NEXAFS spectra of $(TMTSF)_2PF_6$ single crystals. The angular dependence is studied around room temperature while the temperature dependence is followed at normal incidence (θ = 0°). The main results of section III will be discussed in depth later in section V on the basis of first-principles DFT calculations.

Angular Dependence Around Room Temperature. Figure 2 compares the RT spectra of the Se $M_{2/3}$-edges of a $(TMTSF)_2PF_6$ single crystal and of a TMTSF powder. It reveals broad $3p_{1/2}$ and $3p_{3/2}$ core-level signals. The spin-orbit doublet is more clearly resolved in the neutral powder than in the $(TMTSF)_2PF_6$ charge transfer salt, because the peaks are narrower. The $3p_{3/2}$ transition of $(TMTSF)_2PF_6$, is significantly broader than in TMTSF powder and the signal is shifted to lower photon energies. The $3p_{1/2}$ transition is barely visible due to its larger width and since it sits on a steeply dropping background curve. The Se $3p_{1/2,3/2}$ spin-orbit splitting appears increased by about 2.8 eV in $(TMTSF)_2PF_6$.

Figure 3 presents the angular dependent spectra of the F K-edge, C K-edge, P $L_{2/3}$-edges and Se $M_{2/3}$-edges taken for θ = 0°, 20°, 40° and 60° at 260 K. Let us first briefly discuss the results for the PF_6 anion and then for the TMTSF donor.

The F K-edge NEXAFS spectrum exhibits clear peaks at photon energies of 688.2, 693.5 and 697 eV, labelled 1, 2 and 3 in Figure 3a. For $(TMTSF)_2PF_6$ signals 1 and 2 are shifted to higher photon energies than the corresponding signals of $(TMTTF)_2AsF_6$.[12] NEXAFS spectra show a slight variation of the total intensity when θ increases which could be due to the varying photon penetration depth with θ. The positions of the peaks remain unchanged when

θ is varied. Sing at al. [28] obtained similar results for a $(TMTSF)_2PF_6$ single crystal by means of X-ray photoelectron spectroscopy of the F 1s edge.

The P spectrum consists of a well-resolved $2p_{1/2,3/2}$ spin-orbit doublet at energies of 137.8 and 138.8 eV (Figure 3c). The angular sequence shows essentially the same monotonous global intensity variation as found for F K-edge. Note that the L_2/L_3 intensity ratio of the P $L_{2/3}$-edges are inverted with respect to that of the Se $M_{2/3}$-edges (Figure 2). Similarly to the P signal, a reversed L_2/L_3 intensity ratio was previously reported for SF_6.[29] This effect has been explained as being due to exchange between the core hole and the excited electron. Such an effect should be strong for anions, since the excited electron is sizably confined in the "cage" of fluorine atoms so that the overlap with the core hole is large. This process mostly affects transition probabilities, not the line splitting.

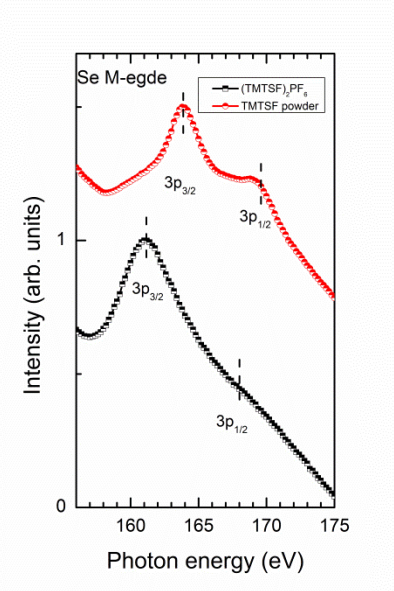

Figure 2. Room temperature NEXAFS spectra of the Se $M_{2/3}$-edges of $(TMTSF)_2PF_6$ single crystal in comparison with TMTSF powder.

In contrast to the F K-edge and P $L_{2/3}$-edges of the PF_6, the C K-edge exhibits a pronounced dependence upon angular variation (Figure 3b). The carbon spectrum is split into three components at photon energies of 283.4, 284.2, and 285.2 eV. Upon increasing θ, the

intensity of the second signal increases while that of the third signal decreases. This is a non-trivial intensity variation which must be connected with the planar orientation of donors in the $(TMTSF)_2PF_6$ structure.

Unlike the S $L_{2/3}$ edges measured in $(TMTTF)_2AsF_6$, the Se $M_{2/3}$-edges of $(TMTSF)_2PF_6$ do not exhibit a well resolved spectrum (Figures 2 and 3d), very likely due to the much shorter lifetime of the Se 3p core hole (Figures 2 and 3d). The possibility of Coster-Kronig or even super-Coster-Kronig decays for Se 3p core holes increases the approximate lifetime width from 0.1 eV for S $L_{2/3}$ to 1.5-2 eV for Se $M_{2/3}$.[30,31] The Se $M_{2/3}$-edges spectrum does not show any significant angular dependence.

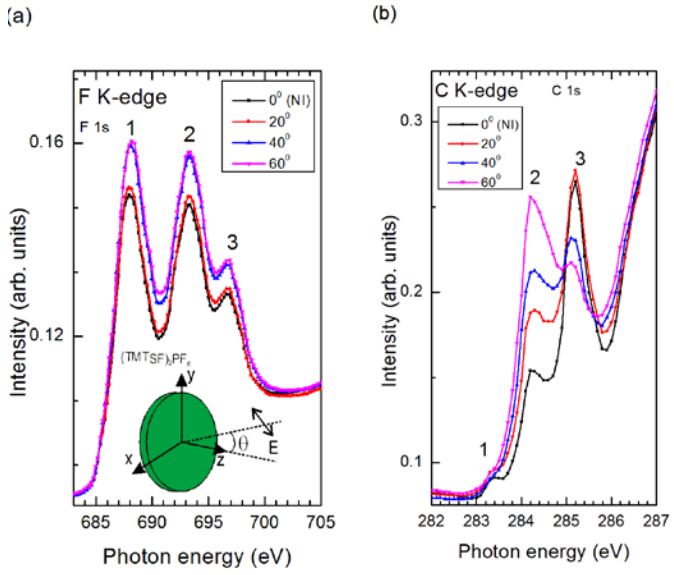

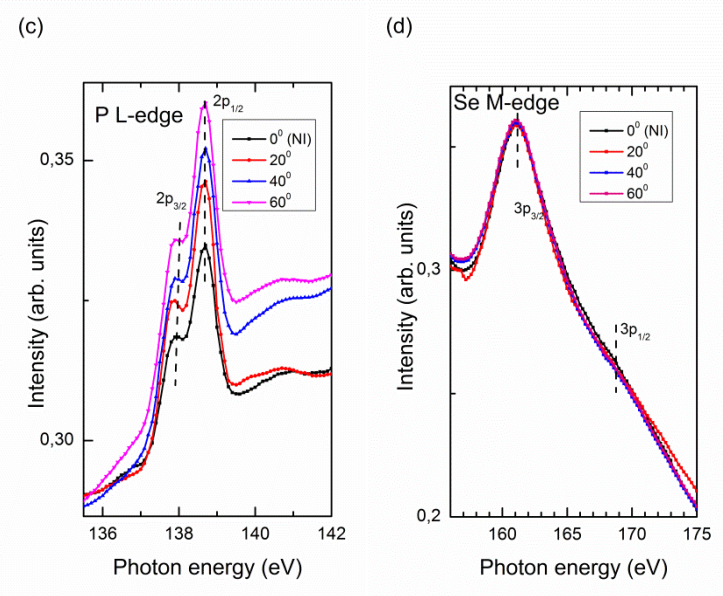

Figure 3. NEXAFS spectra of the F K-edge (a), C K-edge (b), P $L_{2/3}$-edges (c) and Se $M_{2/3}$-edges (d) of a $(TMTSF)_2PF_6$ single crystal as a function of the angle θ between the electric field vector and the surface plane (containing the stack direction, *a*). The inset in (a) shows the experimental configuration.

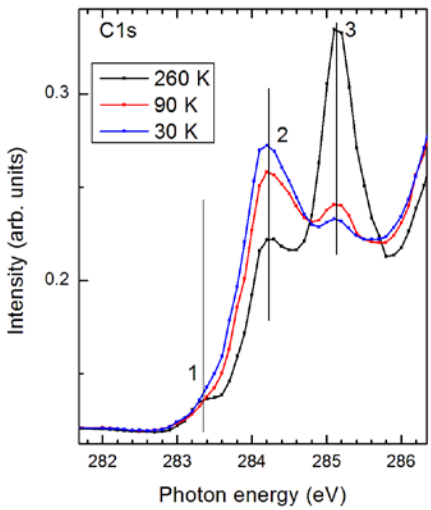

Figure 4. Carbon 1s NEXAFS spectra of $(TMTSF)_2PF_6$ taken at 260, 90 and 30 K in normal incidence.

Temperature Dependence at Normal Incidence. The temperature dependence measurements, reported at 260, 90 and 30 K in this part were obtained at normal incidence where the electric vector of the X-ray beam is aligned along the stack direction *a*.

The C 1s spectrum which consists of three pronounced features exhibits strong temperature dependence (Figure 4). The intensity of peak 2 strongly increases upon cooling while the intensity of peak 3 strongly decreases. Note that the same trend is observed for the angular dependence when θ increases at constant temperature (Figure 3b). No peak shift larger than 0.1 eV (the experimental uncertainty in the determination of the peak position) could be detected upon cooling.

Figure 5 displays the temperature dependence of the F 1s spectrum. Clearly, there is no thermal shift of the peak position upon cooling for any of the three peaks of the spectra. This is in contrast with our previous work on $(TMTTF)_2AsF_6$ where significant shifts were observed as a function of temperature. [12] The intensity of the three peaks does not change appreciably upon cooling. There is however a slight broadening of peaks 1 and 2 upon cooling. Interestingly, the lower energy peak 1 is twice larger than the corresponding peak 1 of $(TMTTF)_2AsF_6$.[12] All these features suggest the presence of one or several additional transitions of weak intensity at energies intermediate between those of peaks 1 and 2. A de-convolution procedure using a multi-peak fit routine provides evidence of such additional transitions. However due to their weakness it was not possible to locate them precisely. Additional transitions giving rise to a four peak F K–edge spectrum was clearly detected in $(TMTTF)_2AsF_6$.[12]

The P $L_{2/3}$-edges spectra (Figure 6) as well as the Se $M_{2/3}$-edges spectra (Figure 7) of $(TMTSF)_2PF_6$ do not show any significant change upon cooling.

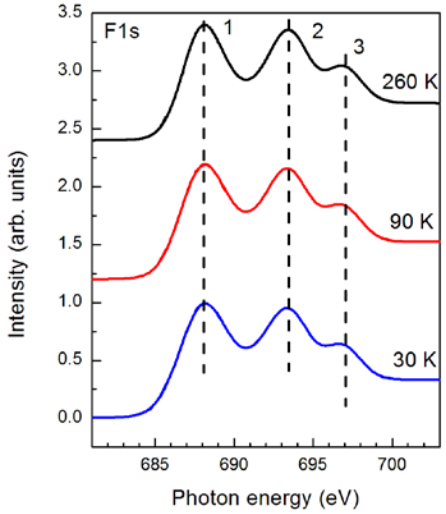

Figure 5. Fluorine 1s NEXAFS spectra of $(TMTSF)_2PF_6$ taken at 260, 90 and 30 K in normal incidence.

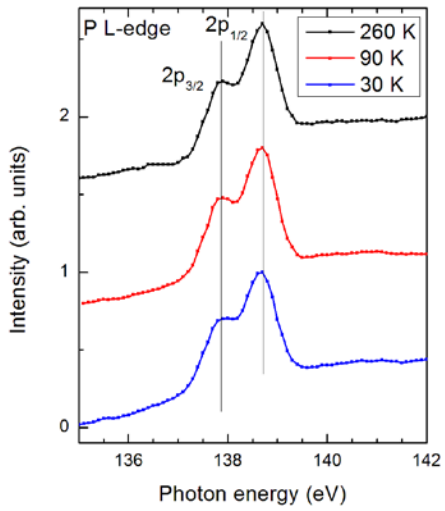

Figure 6. Phosphorous 2p NEXAFS spectra of $(TMTSF)_2PF_6$ taken at 260, 90 and 30 K in normal incidence.

Summary of the NEXAFS Results. The more salient results of our NEXAFS study can be summarized as follows:

(a) The F K-edge spectra consist of three visible peaks which do not exhibit any sizeable temperature dependence. The position of these peaks remains unchanged and only a small

intensity variation occurs when θ, the angle between the light polarization vector and the stack axis *a*, is varied.

(b) The C K-edge spectra contain also three main peaks. These peaks exhibit a strong and non-trivial angular and temperature dependence.

(c) In contrast with a previous studies of the S $L_{2/3}$-edges spectra in $(TMTTF)_2AsF_6$,[12] the Se $M_{2/3}$-edges of $(TMTSF)_2PF_6$ do not exhibit a well resolved spectrum. The spectra do not show any significant angular or temperature dependence.

(d) The P $L_{2/3}$-edges spectrum consists of a well-resolved $2p_{1/2}$ and $2p_{3/2}$ spin-orbit doublet without significant angular or temperature dependence.

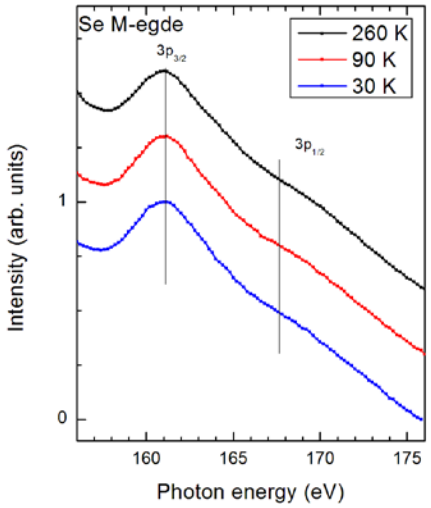

Figure 7. Selenium 2p NEXAFS spectra of $(TMTSF)_2PF_6$ taken at 260, 90 and 30 K in normal incidence.

- **ENERGY LEVELS OF PF_6^-, TMTSF AND $(TMTSF)_2PF_6$**

In previous studies of molecular conductors[12,32] we found that important guidelines to understand their NEXAFS spectra are provided by the analysis of the empty levels of the solid

and those of the associated donor and anion according to first-principles calculations. Here we follow the same approach and report in this section the results of first-principles DFT calculations for metallic $(TMTSF)_2PF_6$, TMTSF donor and PF_6^- anion using the room temperature and 4 K crystal structures. Remarkable differences between the sulfur and selenium bearing $(TMT(T/S)F)_2X$ salts emerge from this study.

A. Energy levels of the PF_6^- anion

The relevant orbitals of the PF_6^- anion are shown in Figure 8. These orbitals are obtained using the geometry of the anion in the crystal structure of $(TMTTF)_2PF_6$ at 4 K[14] and the energy values (in eV) are relative to the energy of the HOMO. In a perfect octahedral environment, the three HOMO, HOMO-1 and HOMO-2 levels would be a degenerate triplet. This is also the case for the three LUMO+1, LUMO+2 and LUMO+3 levels. The LUMO (lowest unoccupied molecular orbital) has as the major component the P 3s orbital which mixes with some F 2p orbitals in an antibonding way. The LUMO+1, LUMO+2 and LUMO+3 levels are strongly antibonding levels composed of the p orbitals of both P and F. In contrast the HOMO, HOMO-1 and HOMO-2 orbitals are really nonbonding because there are no P orbitals of appropriate symmetry to mix with.

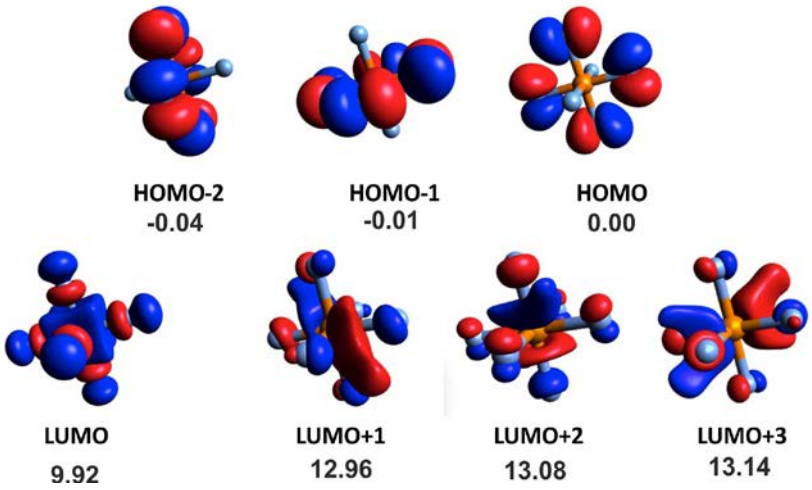

Figure 8. PF_6^- molecular orbitals relevant for the analysis of the NEXAFS spectra of $(TMTSF)_2PF_6$. Energy values (in eV) are given with respect to the energy of the HOMO.

Although the shape of these orbitals is similar to those previously reported for the AsF_6^- anion[12] (see Figure S1 in the supplementary information for a comparison) there is a very significant difference: the energy separation between the LUMO and LUMO+i orbitals is now around 3.1 eV whereas for AsF_6^- the difference obtained with the same computational approach was found to be considerably larger, 4.8 eV. This observation is in agreement with the fact that in our previous work concerning $(TMTTF)_2AsF_6$[12] we attributed peaks 1 and 3 of the F 1s spectra, which were separated by 6.8 eV, to the LUMO and LUMO+i levels of the anion. In the present case (see Figure 5) these levels are associated with peaks 1 and 2 and now the separation is noticeably smaller, 5.3 eV. The larger separation found for the AsF_6^- anion is mostly due to the more extended nature of the As orbitals which overlap better with the F 2p orbitals leading to a larger splitting.

Energy Levels of the TMTSF Donor. The calculated HOMO, LUMO and the next six unoccupied molecular orbitals of TMTSF are shown in Figure 9. The geometry used is based on the 4 K crystal structure of $(TMTSF)_2PF_6$[14] in which the TMTSF molecules were slightly modified so as to exhibit D_{2h} symmetry. The energy values (in eV) are relative to the energy of the HOMO. Although the shape of these orbitals is similar to that of the TMTTF molecules in $(TMTTF)_2AsF_6$[12] (see Figure S2 in the supplementary information for a comparison) the ordering of such levels is clearly different. Whereas four orbitals, HOMO, LUMO, LUMO+2 and LUMO+6, remain in the same relative position in the two salts, three of them change. The LUMO+3, LUMO+4 and LUMO+5 of $(TMTTF)_2AsF_6$ become respectively the LUMO+4, LUMO+1 and LUMO+3 of $(TMTSF)_2PF_6$. The important consequence is that in the present

case it is not possible to separate the five orbitals from LUMO+1 to LUMO+5 into two groups, π and σ, differing by their symmetry with respect to the molecular plane, as it was possible for the TMTTF levels in $(TMTTF)_2AsF_6$[12] or the TTF levels in TTF-TCNQ.[32] In these TTF-based salts there occurs a group of three π type orbitals and then a group of two σ type orbitals (and somewhat higher in energy lies another σ orbital). In the TMTSF salt the energy differences among the five orbitals are smaller and the sequence is σ, π < σ < π < π. The LUMO and LUMO+6 levels remain well separated from the other five levels, as it was the case for $(TMTTF)_2AsF_6$. Thus, we conclude that replacement of Se for S in TMTTF leads to an important electronic rearrangement among the unoccupied molecular orbitals which must become apparent in the NEXAFS spectra.

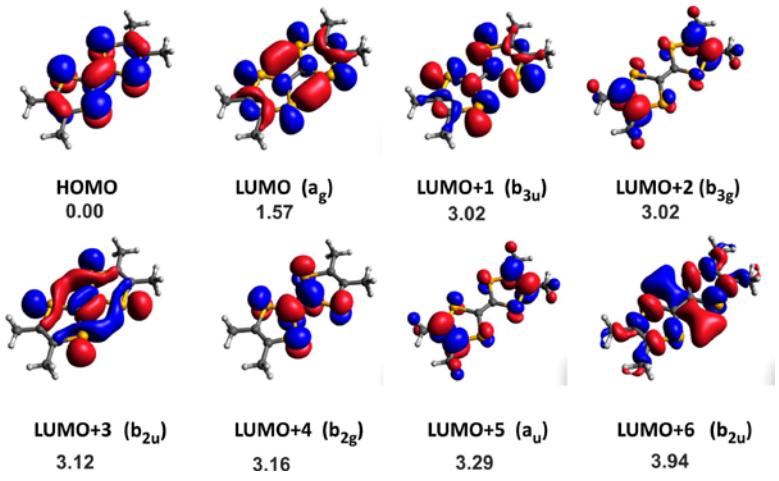

Figure 9. TMTSF molecular orbitals relevant for the analysis of the NEXAFS spectra of $(TMTSF)_2PF_6$. The geometry of TMTSF is based on the 4 K crystal structure of $(TMTSF)_2PF_6$ where the TMTSF donors where symmetrized so as to possess D_{2h} symmetry. Energy values (in eV) are given with respect to the energy of the HOMO.

At this point we note that the energy range in which the five orbitals LUMO+1 to LUMO+5 occur in Figure 9 is 0.27 eV. This is clearly much smaller than the energy range of 0.92 eV obtained in $(TMTTF)_2AsF_6$[12] using exactly the same computational approach for the TMTTF donor. Without entering for the moment into a detailed discussion of the C 1s spectra of $(TMTSF)_2PF_6$, let us remark that the separation between the two main peaks of this spectra (peaks 2 and 3 in Figure 4), which are associated with these levels, is only 0.9 eV in $(TMTSF)_2PF_6$ but 2.3 eV in the C 1s spectra of $(TMTTF)_2ReO_4$[33] and 2.25 eV in the S 2p spectra of $(TMTTF)_2AsF_6$.[12] Consequently, the theoretically predicted narrowing of the energy range where the five levels from LUMO+1 to LUMO+5 occurs, seems well justified from the available NEXAFS information. Such a narrowing is obviously in favor of the occurrence of different level orderings among the unoccupied orbitals of the TMTTF and TMTSF salts.

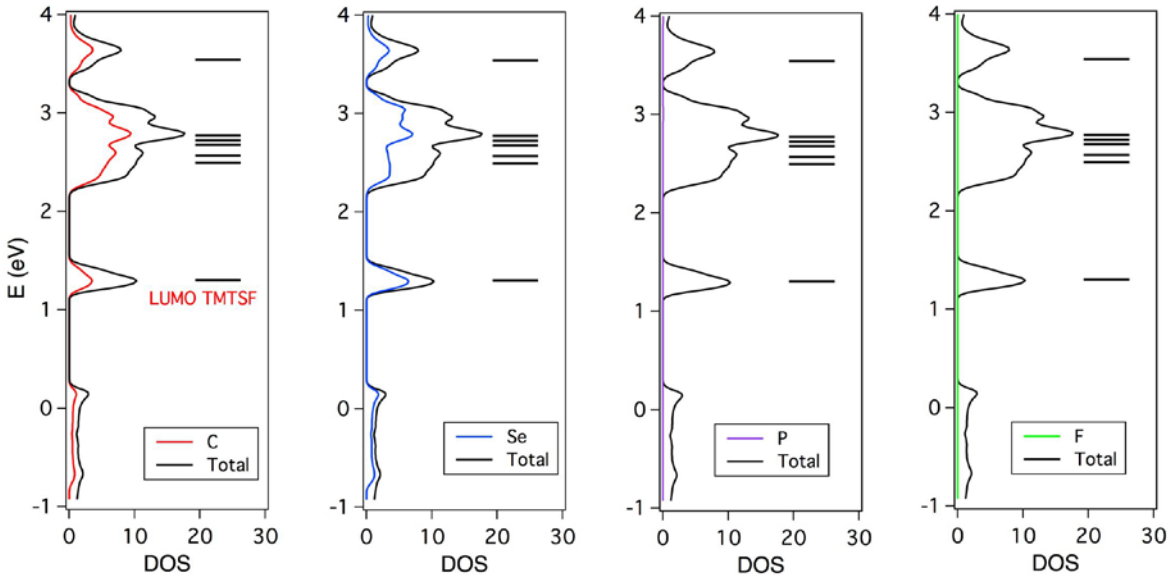

Figure 10. Total DOS and local projections (PDOS) of the contributions of the C, Se, P and F atoms calculated for $(TMTSF)_2PF_6$. The molecular energy levels of TMTSF are also included. The energy zero is the Fermi level.

Energy Levels of Metallic $(TMTSF)_2PF_6$. Figure 10 shows the calculated density of states (DOS) for $(TMTSF)_2PF_6$ using the 4 K crystal structure as well as the separate contribution of the C, Se, P and F orbitals. We report in Figure 11 the decomposition of the partial DOS of the C and Se atoms into σ and π type contributions. The calculated discrete levels of TMTSF at the same temperature are also shown in these figures where the LUMO orbital has been aligned with the corresponding peak in the DOS. If these results are compared with those previously reported for $(TMTTF)_2AsF_6$,[12] two features are surprising. First, no P or F levels occur within the whole energy range of the LUMO to LUMO+6 levels of TMTSF. This means that the LUMO of PF_6^- is now located at higher energies. This is very different from the case of $(TMTTF)_2AsF_6$ where the LUMO of AsF_6 was practically aligned with the LUMO+1 of the donor. The origin of this important difference is that the *d* orbitals of Se are considerably more spread and thus, the interaction between the TMTSF and PF_6^- molecular orbitals is considerably stronger so that the PF_6^- levels are pushed quite high in energy. Second, it is clear from Figure 11 that, as already discussed for the isolated TMTSF molecule, in the solid there is not a clear separation between σ and π levels of TMTSF. This will render the interpretation of the NEXAFS spectra more complex.

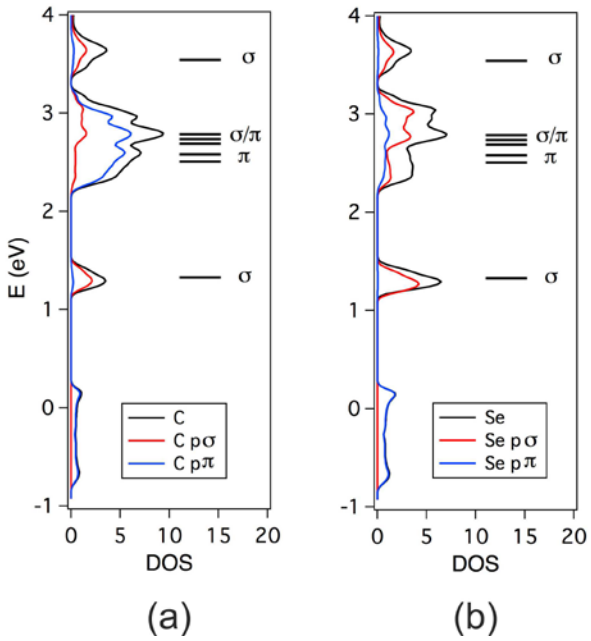

Figure 11. Decomposition of the contributions of the C (a) and Se (b) to the DOS of $(TMTSF)_2PF_6$ into σ (red) and π (blue) type components. The molecular energy levels of TMTSF are also included.

Se for S Replacement Has a Strong Effect on the Empty Donor Levels of $(TMT(T/S)F)_2X$ Salts. Although the previous discussion makes clear that the Se for S substitution in TMTTF must induce quite important modifications in the NEXAFS spectra of their conducting salts, there is an important aspect of our calculations that we still have not discussed. When the molecular orbitals of the discrete TMTSF molecule are calculated without any symmetrization, i.e. using exactly the same geometry that they exhibit in the 4 K or room temperature crystal structures (see Figures S3 and S4 in the Supplementary Information), several of the LUMO+i orbitals of TMTSF noticeably depart from the clear σ or π separation of orbitals in the symmetrized model (Figure 9). Indeed, these orbitals can be expressed as a combination of orbitals of the two symmetries. This feature is due to the fact that the TMTSF donors are not exactly planar in the real crystal structure. Although the non-planarity is relatively weak and the effect is practically nil for the LUMO and all the occupied

orbitals, it has a non-negligible effect (Figures S3 and S4 in supplementary information) for the LUMO+i orbitals. The reason for which this happens is that these orbitals are located exactly in the same energy region as the *d* orbitals of Se which, being much extended, couple orbitals of quite distant atoms within the molecule. We have verified that the same effect occurs in TMTTF although, but since the S *d* orbitals are considerably less extended, which leads to a weaker coupling strength, the non-planarity effect really does not influence the results in a perceptible way in that case.

Essentially, the above observations mean that replacement of Se for S in the molecular network of the TMTTF donors leads to a strong intermingle of σ and π type components of the molecular levels in the region of the LUMO+1 to LUMO+5 orbitals, i.e. those responsible for the stronger peaks in the C 1s spectra. Since the geometry of the TMTSF donor varies with temperature, the proportion of the two components may change in the spectra at different temperatures. Thus, as the temperature variation may affect both the separation of the different levels and the mixing of σ and π components, it is difficult to have some guideline to understand the temperature evolution of the C 1s spectra (Figure 4). Yet, this is a crucial aspect to settle the differences between the Fabre (i.e. sulfur-containing) and Bechgaard (i.e. selenium-containing) $(TMT(T/S)F)_2X$ salts.

In order to have some hint of the intrinsic behavior of the donor we have taken the different TMTSF levels calculated for the discrete molecules using their geometry in the crystal structures at room temperature and 4 K and constructed TMTSF DOS with an appropriate Gaussian smoothing (as used for solid state calculations) at the two temperatures and projected the σ and π type contributions. The results are shown in Figure 12. These results suggest two important guidelines: (1) the σ and π contributions are more evenly distributed at room temperature, and (2) when lowering the temperature the π/σ levels tend to concentrate more strongly in the lower/higher energy levels. In contrast, no major changes

occur for TMTTF when the same model calculations are carried out using the room temperature and low temperature (4 K) crystal structures of $(TMTTF)_2AsF_6$ (Figure S5 in supplementary information).

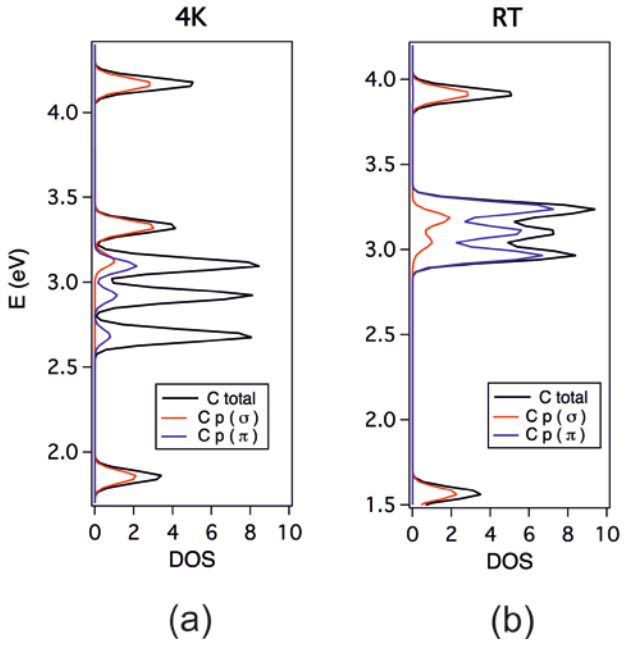

Figure 12. Projection of the σ (red) and π (blue) contributions of the 2*p* orbitals of C to the "DOS" of discrete TMTSF levels calculated using the crystal structure of $(TMTSF)_2PF_6$ at 4 K (a) and room temperature (b). Energies (in eV) are relative to the energy of the HOMO.

Summary of the DFT Calculations. Noteworthy results of the DFT study differing from previous work on the sulphur based TMTTF salts are:

(a) The energy separation between the LUMO and the three LUMO+i orbitals of PF_6^- is considerably smaller (around 1.7 eV) than in AsF_6^-.

(b) Replacement of Se for S in TMTTF and the slight non-planarity of TMTSF in the $(TMTSF)_2PF_6$ salt lead to an important rearrangement of the unoccupied molecular orbitals:

they cannot be considered anymore as pure σ or π type levels and, even taking into account this fact, they cannot be separated in blocks of mostly σ and mostly π type orbitals.

(c) When lowering the temperature the π contributions tend to concentrate in the lower-lying empty orbitals whereas the opposite occurs for the σ contributions.

- **DISCUSSION OF THE NEXAFS SPECTRA OF $(TMTSF)_2PF_6$**

On the basis of the above DFT results and our previous analysis of the NEXAFS spectra of the related $(TMTTF)_2AsF_6$ salt[12] we can now discuss the experimental results for $(TMTSF)_2PF_6$, and more specially those of the C 1s and F 1s spectra. Let us remind that the NEXAFS transitions probe the unoccupied orbital structure which spatially overlaps with the initial-state orbital, in our case C 1s and Se 2p in the donor moiety and P 2p and F 1s in the anion. Besides the orbital overlap, the matrix element of the photon operator sorts out the proper angular momenta via the dipole selection rules ($\Delta l = \pm 1$) and the polarization effects due to the orientation of the linearly polarized photon beam.

C 1s spectra: Angular and Temperature Evolution. The C 1s spectra (Figures 3b and 4) exhibit three distinctive peaks. The first and smaller one (labeled 1 in Figure 4) is easily assigned to the σ type LUMO of TMTSF. Then, there are two peaks (labeled 2 and 3 in Figure 4) displaying a puzzling behavior when both the temperature and θ dependences are considered. The intensity of peak 2 increases when either the temperature decreases or θ increases. Peak 3 follows an opposite behavior. Measurements were carried out with an orientation such that the electric field vector is parallel to the TMTSF stacking direction when the incoming beam is normal to the sample (θ = 0°) but perpendicular to this direction for θ = 90°. Thus, for values of θ around 0°, there are the π type levels which are mostly probed. When the sample is tilted the contribution of the π empty states is reduced whereas that of the

empty σ states is enhanced. Looking at Figure 3b it is clear that the intensity of the second peak is strongly enhanced with θ so that this peak, which contains both σ and π type TMTSF contributions, should be dominated by the σ type states. In contrast, the third peak, exhibiting the opposite θ dependence, which contains both σ and π type TMTSF contributions should be dominated by the π type states. Note that the small peak 1 which slightly increases in intensity with θ which corresponds to a σ type orbital (LUMO). The contribution of the σ type LUMO+6 most likely overlap with the strong absorption occurring around 286 eV.

To understand the temperature dependence of the spectra (Figure 4) we must remind that the π levels tend to concentrate in the lower energy levels when the temperature decreases. This provides a simple rationalization for the intensity increase of peak 2 which according to the θ dependence should be dominated by σ levels at room temperature. For the same reason, the intensity decrease of peak 3 is easily understandable because it is dominated by π levels at room temperature. Consequently, we suggest that the σ and π type levels associated with the LUMO+1 to LUMO+5 of TMTSF (Figure 9) experience a complex redistribution as a function of temperature, something which strongly contrasts with the case of the $(TMTTF)_2AsF_6$ salt.[12] In the latter case the nature of the different peaks remains constant for all temperatures even if their intensity evolves as a result of the charge localization phenomenon and the charge ordering transition.

F 1s spectra: Differences with the $(TMTTF)_2AsF_6$ Salt. As noted above, an important difference with the $(TMTTF)_2AsF_6$ salt is that the first and second peaks of the F 1s spectra (Figure 5) occur now around 3 and 2.5 eV higher in energy than peaks 1 and 3 (i.e. the most intense ones) in $(TMTTF)_2AsF_6$. Thus, it appears that there is a positive shift of the spectra. In addition, peak 1 in the present salt is noticeably broader than in $(TMTTF)_2AsF_6$. Let us briefly consider the contribution of the anion levels to the calculated DOS in order to trace back the

origin of these differences (see Figure 13a). This contribution is quite different from that previously found in the $(TMTTF)_2AsF_6$ salt. In the present case there is a very broad and continuous contribution of the PF_6 projected DOS with two peaks centered at around 6.6 and 10.2 eV. Note that the ratio of the integrated projected DOS associated with the two peaks is ~1/3 so that these two peaks are associated with the LUMO and the three LUMO+i levels of the PF_6^- anion (see Figure 8). The contribution of the LUMO+i levels was also found quite broad for $(TMTTF)_2AsF_6$ but the contribution of the LUMO was found to be narrow. In addition the lower peak is centered now at around 6.6 eV from the Fermi level which is approximately 4 eV higher than in $(TMTTF)_2AsF_6$ (see Figure 7b in reference 12). This is in good agreement with the above mentioned shift of the first peak in the F 1s spectra of the two salts. We thus conclude that the first peak originates from the anion LUMO level and that peaks 2 and 3 must be associated to the LUMO+i levels.

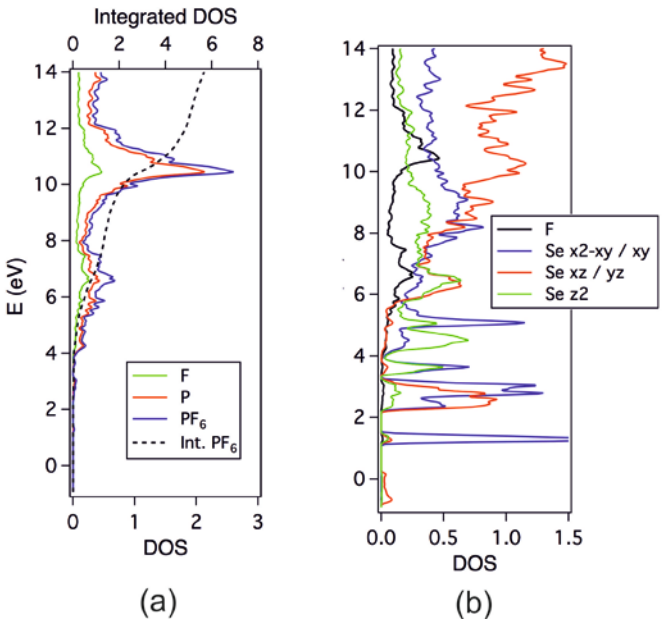

Figure 13. (a) Projection of the PF_6 (blue), P (red) and F (green) contributions to the DOS of $(TMTSF)_2PF_6$. The dashed black line is the integrated contribution of PF_6 above the Fermi

level. (b) Se *d* orbital and F contributions to the DOS of $(TMTSF)_2PF_6$. Note that the DOS scale in (b) is smaller.

Before considering more in depth the F 1s spectra let us examine the reason for the shift as well as the broad nature of the contribution of all empty levels of PF_6^-. Figure 13b shows the projected Se *d* orbitals in the region of the empty states of $(TMTSF)_2PF_6$. The chalcogen *d* orbitals contribution is considerably stronger than it was in the $(TMTTF)_2AsF_6$ salt. The important observation which can be made from this figure is that all along the DOS region with F contributions there is also Se *d* orbitals participation. This is specially the case in the region of the LUMO+i levels. This means that there is a strong interaction between donor and anion empty levels mostly mediated by the F 2*p*···Se 4*d* interactions through the short F···Se contact distances shown in Figure 1b, and that this affects more strongly the LUMO+i. The first consequence of this strong interaction is that the LUMO and LUMO+i orbitals of the anion are pushed to considerably higher energies than in $(TMTTF)_2AsF_6$, as clearly shown by the F 1s spectra. The second consequence is that both the LUMO and LUMO+i levels, but more specially the last ones, become very broad leading to a continuous contribution of more than 10 eV as probed in the F 1s spectra (Figure 3a). The LUMO+i levels lead to the strong peak 2, the somewhat higher lying peak 3 and most likely to another sizeable contribution at lower energies overlapping with part of peak 1. Because of the strength of the interactions and the overlap of contributions, a de-convolution of the F 1s spectra, as carried out in our previous study of $(TMTTF)_2AsF_6$ would not be very insightful in the present case. In addition, the temperature dependence of the spectra does not exhibit any noticeable displacement of the peaks. All these observations are consistent with a description of the F 1s spectra with two main contributions, peak 1 (LUMO) and peaks 2 and 3 (LUMO+i) considerably broadened because of the large mixing of donor-anion levels through the F 2*p*···Se 4*d* interactions. Also,

the small temperature variation indicates some reorganization within the very broad energy range associated with the F 2*p*···Se 4*d* interactions but without noticeable variation of the main peaks. This broadness is most likely the reason for the fact that we did not find any evidence in NEXAFS spectra of the freezing of the PF_6-librational motion in the methyl group cavity or of the methyl group thermal rotational disorder.

Absence of Angular Dependence of the P $L_{2/3}$-Edges and Se $M_{2/3}$-Edges Spectra. In view of the very isotropic nature of the combination of three LUMO+i orbitals and the nature of the HOMO (of a_1 type symmetry) of the PF_6 no significant changes should be expected in the P 2p spectra for measures at different θ values even if the P *d* orbitals are taken into account. The same conclusion applies to the F 1s spectra.

Coming back to Figure 13b, note that all along the Se *d* orbitals contribution, there is a strong overlap of *d* orbitals in the plane of the TMTSF molecules (x^2-y^2, xy: blue line) and *d* orbitals perpendicular to this plane (z^2, xz, yz: red and green lines). This confers a quite isotropic nature to the Se *d* contribution consistent with the practically nil angular dependence of the Se M_2/M_3-edges spectra (Figure 3).

- **CONCLUDING REMARKS.**

High-resolution NEXAFS spectra at the P $L_{2/3}$-edges, F K-edge, C K-edge and Se $M_{2/3}$-edges have been used to probe the nature of the unoccupied levels of the $(TMTSF)_2PF_6$ quasi-1D molecular conductor and superconductor and the results have been discussed on the basis of first-principles DFT calculations. Despite the structural similarity, the NEXAFS spectra of $(TMTSF)_2PF_6$ and $(TMTTF)_2AsF_6$ exhibit very remarkable differences:

(i) The donor-anion interactions are stronger in the Se-based salt $(TMTSF)_2PF_6$ than in $(TMTTF)_2AsF_6$ because the whole F K-edge spectrum is globally shifted towards higher

energies (and towards lower energies for the C1s if our results are compared with the available XANES data[33] of $(TMTTF)_2ReO_4$).

(ii) The donor-anion interactions do not appreciably change with temperature for $(TMTSF)_2PF_6$ whereas they do considerably for $(TMTTF)_2AsF_6$. This is a very significant feature clearly illustrated by NEXAFS and related with the different phase diagram of the two materials. The thermal increase of the donor-anion interactions in the TMTTF salts is intimately related with its progressive charge localization upon cooling. In contrast, the enhanced interaction between the conduction electrons and the anions in the TMTSF salts is however smoothed because of the more 2D electronic structure and the more polarizable nature of TMTSF. This is at the basis of the different NEXAFS results for the two salts.

(iii) The selenium for sulfur replacement in the TMTTF donor induces an important reorganization of the empty molecular orbitals of the system which leaves practically unaffected the occupied and LUMO donor orbitals. Such reorganization induces some σ/π mixing in these empty levels such that a combined study of the angular and temperature dependence is required in order to fully characterize them. This is in striking contrast with the situation in the sulfur TTF based salts like those of TMTTF[12,33] of TTF,[32,34] where the temperature dependence already allows a full characterization.

■ ASSOCIATED CONTENT

[*S] Supporting Information

Theoretical calculations of the molecular orbitals relevant for the analysis of the NEXAFS spectra of $(TMTSF)_2PF_6$.

This material is available free of charge via the Internet at http://pubs.acs.org.

■ AUTHOR INFORMATION

Corresponding Author

*E-mail: medyanyk@uni-mainz.de Phone: +4961313923629 Fax: +4961313923807.

Notes

The authors declare no competing financial interest.

▪ ACKNOWLEDGMENTS

Work in Spain was supported by MINECO (Spain) through Grants FIS2012-37549-C05-05, FIS2015-64886-C5-4-P and CTQ2015-64579-C3-3-P, and Generalitat de Catalunya (2014SGR301 and XRQTC). E.C. acknowledges support of the Spanish MINECO through the Severo Ochoa Centers of Excellence Program under Grant SEV-2015-0496. Special thanks are due to Graduate School of Excellence MAINZ and to Transregio SFB TR49. The crystals were synthesized by the late A. Moradpour. We would like to thank to MAX IV laboratory for providing beam time at I1011 beam line.

▪ REFERENCES

(1) Jérome, D.; Mazaud, A.; Ribault, M.; Bechgaard, K. Superconductivity in a synthetic organic conductor $(TMTSF)_2PF_6$. *J. Phys. Lett. (Paris)* **1980**, *41*, L-95.

(2) *Physics of Organic Conductors and Superconductors*, edited by Lebed, A.G. Springer Series in Materials Sciences (Springer-Verlag, Berlin, Heidelberg, 2008), *Vol. 110*.

(3) Moret, R.; Ravy, S.; Pouget, J.-P. ; Comès, R.; Bechgaard, K. Anion-Ordering Phase Diagram of Di(tetramethyltetraselenafulvalenium) Perrhenate, $(TMTSF)_2ReO_4$. *Phys. Rev. Lett*. **1986**, *57*, 1915-1918.

(4) Alemany, P.; Pouget, J.-P.; Canadell, E. Electronic structure and anion ordering in $(TMTSF)_2ClO_4$ and $(TMTSF)_2NO_3$: A first-principles study. *Phys. Rev. B*, **2014**, *89***,** 155124.

(5) Jérome, D.; Schulz, H. Organic conductors and superconductors. *Adv. Phys.*, **1982**, *31***,** 299-490.

(6) Schwartz, A.; Dressel, M.; Grüner, G.; Vescoli, V.; Degiorgi, L.; Giamarchi, T. On-chain electrodynamics of metallic $(TMTSF)_2X$ salts: Observation of Tomonaga-Luttinger liquid response. *Phys. Rev. B,* **1998**, *58,* 1261-1271.

(7) Moser, J.; Gabay, M.; Auban-Senzier, P.; Jérome, D.; Bechgaard, K.; Fabre, J.M. Transverse transport in $(TM)_2X$ organic conductors: possible evidence for a Luttinger liquid. *Eur. Phys. J. B,* **1998**, *1*, 39-46.

(8) Pashkin, A.; Dressel, M.; Hanfland, M.; Kuntscher, C. A. Deconfinement transition and dimensional crossover in the Bechgaard-Fabre salts: Pressure- and temperature-dependent optical investigations. *Phys. Rev. B,* **2010**, *81*, 125109.

(9) Foury-Leylekian, P.; Petit, S.; Mirebeau, I.; André, G.; de Souza, M.; Lang, M.; Ressouche, E.; Moradpour, A.; Pouget, J.-P. Low-temperature structural effects in the $(TMTSF)_2PF_6$ and AsF_6 Bechgaard salts. *Phys.Rev. B,* **2013**, *88*, 024105.

(10) Coulon, C.; Foury-Leylekian P.; Fabre, J.-M.; Pouget, J.-P. Electronic instabilities and irradiation effects in the $(TMTTF)_2X$ series. *Eur. Phys. J. B,* **2015**, *88*, 85.

(11) Bourbonnais, C.; Jérome, D. Electronic confinement in organic metals. *Science,* **1988**, *281*, 1155- 1156.

(12) Medjanik, K.; Chernenkaya, A.; Nepijko, S. A.; Öhrwall, G.; Foury-Leylekian, P.; Alemany, P.; Canadell, E.; Schönhense, G.; Pouget, J.-P. Donor–anion interactions at the charge localization and charge ordering transitions of $(TMTTF)_2AsF_6$ probed by NEXAFS. *Phys. Chem. Chem. Phys,* **2015**, *17*, 19202-19214.

(13) Medjanik, K.; de Souza, M.; Kutnyakhov, D.; Gloskovskii, A.; Müller, J.; Lang, M.; Pouget, J.-P.; Foury-Leylekian, P.; Moradpour, A.; Elmers, H.-J.; Schönhense G. Hard X-ray photoemission study of the Fabre salts $(TMTTF)_2X$ ($X=SbF_6$ and PF_6) *Eur. Phys. J. B,* **2014**, *87*, 256.

(14) Gallois, B.; Gaultier, J.; Hauw, C.; Lamcharfi, T.; Filhol, A. Neutron low-temperature (4 and 20 K) and X-ray high-pressure (6.5 x 10^2 and 9.8 x 10^2 MPa) structures of the organic superconductor di(2,3,6,7-tetramethyl-1,4,5,8-tetraselenafulvalenium) hexafluorophosphate, $(TMTSF)_2PF_6$. *Acta Crystallogr. Sect. B,* **1986**, *42*, 564-575.

(15) Granier, T.; Gallois, B.; Ducasse, L.; Fritsch, A.; Filhol, A. 4 K crystallographic and electronic structures of $(TMTTF)_2X$ salts (X^-: PF_6^-, AsF_6^-). *Synth. Met.* **1988**, *24*, 343-356.

(16) Kowalik, I. A.; Öhrwall, G.; Jensen, B. N.; Sankari, R.; Wallén, E.; Johansson, U.; Karis, O.; Arvanitis, D. Description of the new I1011 beamline for magnetic measurements using synchrotron radiation at MAX-lab. *J. Phys.: Conf. Ser.*, **2010**, *211*, 012030.

(17) Hohenberg, P.; Kohn, W. Inhomogeneous electron gas. *Phys. Rev.*, **1965**, *136*, B864-B871.

(18) Kohn, W.; Sham, L. J. Self-consistent equations including exchange and correlation effects. *Phys. Rev.*, **1965**, *140*, A1133-A1138.

(19) Soler, J. M.; Artacho, E.; Gale, J. D.; García, A.; Junquera, J.; Ordejón, P.; Sánchez-Portal, D. The SIESTA method for ab initio order-N materials simulation. *J. Phys.: Condens. Matter.*, **2002**, *14*, 2745-2779.

(20) Artacho, E.; Anglada, E.; Diéguez, O.; Gale, J. D.; García, A.; Junquera, J.; Martin, R. M.; Ordejón, P.; Pruneda, J. M.; Sánchez-Portal, D.; Soler J. M. The SIESTA method; developments and applicability. *J. Phys.: Condens. Matter.*, **2008**, *20*, 064208.

(21) For more information on the SIESTA code visit: http://departments.icmab.es/leem/siesta/

(22) Perdew, J. P.; Burke, K.; Ernzerhof, M. Generalized gradient approximation made simple. *Phys. Rev. Lett.*, **1966**, 77, 3865-3868.

(23) Troullier, N.; Martins, J. L. Efficient pseudopotentials for plane-wave calculations. *Phys. Rev. B*, **1991**, *43*, 1993-2006.

(24) Kleinman, L.; Bylander D. M. Efficacious form for model pseudopotentials. *Phys. Rev. Lett.*, **1982**, *48*, 1425-1428.

(25) Artacho, E.; Sánchez-Portal, D.; Ordejón, P.; García, A.; Soler, J. M. Linear-scaling ab-initio calculations for large and complex systems. *Phys. Stat. Sol. (b)*, **1999**, *215*, 809-817.

(26) Monkhorst, H. J.; Pack J. D. Special points for Brillouin-zone integrations. *Phys. Rev. B*, **1976**, *13*, 5188-5192.

(27) Thorup, N.; Rindorf, G.; Soling, H.; Bechgaard, K. The structure of di (2, 3, 6, 7-tetramethyl-1, 4, 5, 8-tetraselenafulvalenium) hexafluorophosphate,$(TMTSF)_2PF_6$, the first superconducting organic solid. *Acta Crystallogr. B*, **1981**, *37*, 1236-1240.

(28) Sing, M.; Schwingenschlögl, U.; Claessen, R.; Dressel, M.; Jacobsen, C. S. Surface characterization and surface electronic structure of organic quasi-one-dimensional charge transfer salts. *Phys. Rev. B*, **2003**, *67*, 125402.

(29) Hudson, E.; Shirley, D. A.; Domke, M.; Remmers, G.; Puschmann, A.; Mandel, T.; Xue, C.; Kaindl, G. High-resolution measurements of near-edge resonances in the core-level photoionization spectra of SF_6. *Phys. Rev. A*, **1993**, *47*, 361-373.

(30) Keski-Rahkonen, O.; Krause M. O. *Atomic Data and Nuclear Data Tables*, **1974,** *14*, 139–146.

(31) Campbell, J. L.; Papp T. *Atomic Data and Nuclear Data Tables*, **2001**, *77*, 1-56.

(32) Fraxedas, J.; Lee, Y. J.; Jiménez, I.; Gago, R.; Nieminen, R. M.; Ordejón, P.; Canadell, E. Characterization of the unoccupied and partially occupied states of TTF-TCNQ by XANES and first-principles calculations. *Phys. Rev. B*, **2003**, *68*, 195115.

(33) Subías, G.; Abbaz, T.; Fabre, J. M.; Fraxedas, J. Characterization of the anion-ordering transition in $(TMTTF)_2ReO_4$ by x-ray absorption and photoemission spectroscopies. *Phys. Rev. B*, **2007**, *76*, 085103.

(34) Chernenkaya, A.; Medjanik, K.; Nagel, P.; Merz, M.; Schuppler, S.; Canadell, E.; Pouget, J.-P.; Schönhense, G. Nature of the empty states and signature of the charge density wave instability and upper Peierls transition of TTF-TCNQ by temperature-dependent NEXAFS spectroscopy. *Eur. Phys. J. B*, **2015**, *88*, 13.